Journal of Applied Polymer Science

Micro-Nanostructured Silicone-Carbon Composite Coatings with Superhydrophobicity and Photoluminescence Prepared by Oxidative Chemical Vapor Deposition

Zhimei Shen, Chengcheng Hou, Shishuai Liu, Zisheng Guan
College of Materials Science and Engineering, Nanjing University of Technology, Nanjing 210009, People's Republic of China
Correspondence to: Z. Guan (E-mail: zsguan@njut.edu.cn)

ABSTRACT: Transparent, superhydrophobic, and colored silicone–carbon composite coatings were prepared by oxidative chemical vapor deposition (oCVD) of bulk silicone at ambient pressure. The colors, wettability, morphologies, and transparency of the coatings can be easily varied via changing both the concentration of gaseous oxygen and the deposition temperature. Typically, the black, brown, and yellow silicone–carbon composite coatings with different superhydrophobicity and transparency were achieved under oxygen-deficient atmospheres. Furthermore, the colored samples showed photoluminescence when they were excited by ultraviolet (UV) light, which is due to the fluorescence of carbons embedded inside the as-prepared coatings. In addition, more regular papillae and nanofibers with excellent superhydrophobicity were obtained at higher deposition temperatures. Our method was believed to develop a new strategy for fabricating multifunctional silicone–carbon composite coatings. © 2014 Wiley Periodicals, Inc. J. Appl. Polym. Sci. **2014**, *131*, 40400.

KEYWORDS: superhydrophobic coatings; silicone-carbon composite; photoluminescent carbon; colors; oxidative chemical vapor deposition

Received 21 November 2013; accepted 4 January 2014
DOI: 10.1002/app.40400

INTRODUCTION

Micro-nanostructured surfaces with unique properties such as robust water-repellency,[1–5] antireflectivity,[6–9] and colors[10–12] have attracted considerable attention in both academia and industry. Recently, polyorganosiloxane has become widely used in fabrication of transparent or antireflective superhydrophobic films, which demonstrate low surface energy, thermal stability, anti-permeability, environmental friendliness, and excellent waterproofing.[13–17] Generally, three approaches have been extensively developed to fabricate superhydrophobic films by using organosilanes. The first one is to use organosilane-modified silica particles to prepare superhydrophobic surface. For example, Li et al.[18] produced a superhydrophobic antireflective film on glass substrates by a layer-by-layer process where mesoporous silica nanoparticles with different sizes were deposited, and finally coated by 1H,1H,2H,2H-perfluorooctyltriethoxysilane using chemical vapor deposition (CVD). Almost perfect superhydrophobic surface was reported by Zhang et al.,[19] where the superhydrophobic coatings were obtained by dip-coating of silica nanoparticles, followed by CVD of silicone nanofilaments. The second route is to develop patterns on silicone rubber. Givenchy et al.[20] generated a PDMS with a superhydrophobic surface by the combination of an acid corrosion followed by the covalent grafting of a highly fluorinated monolayer. Zimmermann et al.[21] also prepared a superhydrophobic surface based on silicone substrates by the combination of an activation in oxygen plasma to generate reactive OH-groups on the surface followed by the functionalized silanes treatment to yield self-assembled monolayers. The third one is to take advantage of hydrolysis and polycondensation of organosilanes to form superhydrophobic nanocoatings. Gao et al.[22] developed a perfect hydrophobic surface on a silicon wafer by using trichloromethylsilane (TCMS). A nanoscale network structure was formed due to the phase separation of a toluene-swollen covalently attached methylsilicone. Superhydrophobic coatings consist of polymethylsilsesquioxane nanofilaments were produced by Artus et al.[23] via the reaction of equimolar amounts of liquid TCMS and water vapor. The simple CVD method could be applied on different substrate materials but the mechanical stability of the coatings was poor. Artus et al.[24] later developed a scale-up of a gas-phase reaction chamber for coating different materials with silicone nanofilaments and rendering them thereby superhydrophobic. Currently, a lot of pure organosilanes are available. However, most organosilanes are extremely reactive, for instance, FAS and chlorosilane. It is difficult to control the reaction conditions and the special equipments are also needed. In

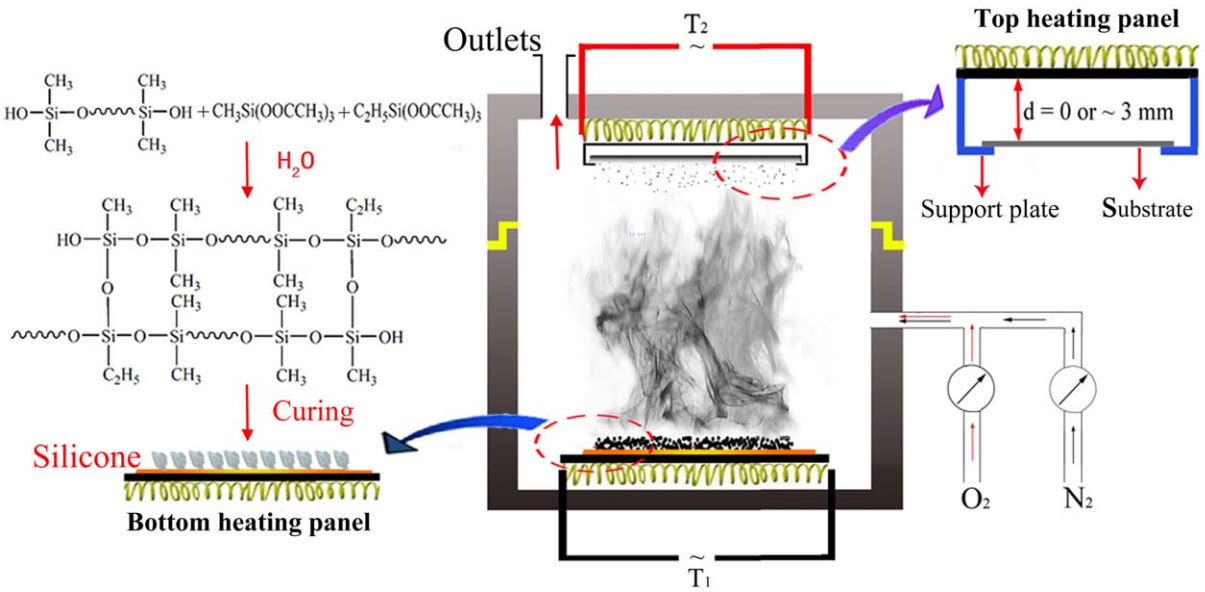

Scheme 1. Illustration for the experimental setup of the preparation of the coatings. [Color figure can be viewed in the online issue, which is available at wileyonlinelibrary.com.]

addition, some reactive organosilanes are expensive, and toxic organic solvents have to be used to disperse organosilanes well. Therefore, more green method at low cost needs to be developed to prepare the superhydrophobic coatings. Here, we use cheap bulk silicone as raw material and fabricate superhydrophobic silicone–carbon composite coatings with multifunction by a facile oCVD method. Bulk silicone is obtained by an important raw material of silicone sealant. In air, the silicone sealant is easily solidified by hydrolysis and copolymerization of the α,ω-dihydroxyl polydimethylsiloxane, methyltriacetoxysilane (MTAS), and ethyltriacetoxysilane (ETAS) to form bulk silicone with network structures. However, the network structures can only be stable at lower temperature, and could be decomposed at higher temperatures.[25–27] The preparing procedure consists of two processes. First, the bulk silicone is primarily decomposed or vapored at high temperature. Second, the decomposed components and silicone vapor are again oxidative decomposed, and then the resulting silicone–carbon composite nanoparticles deposited on the substrates to form coatings at higher temperature under ambient pressure. Moreover, the wettability, morphologies, and optical properties can be easily tuned by varying deposition parameters such as the oxidative deposition temperature, and the concentration of gaseous oxygen. Generally speaking, we prepared a superhydrophobic surface with multifunctional properties, such as transparency, colors, and fluorescence, which would be expected to find applications in optoelectronic fields and facilitate the practical applications of the non-wetting surfaces.

EXPERIMENTAL

Materials

The bulk silicone was obtained by solidification of the Dow Corning® GP Silicone sealant (Dow Corning, America) in air for 7 days at room temperature, whose major components are α,ω-dihydroxyl polydimethylsiloxane, MTAS, ETAS, silicone oil, and silica. Both the glass substrate (76 mm × 25.4 mm × 1.2 mm, Sail Brand, China) and the iron blade (45 mm × 20 mm × 1 mm, Shanghai Zhengli Blade, China) were treated by immersing in a piranha solution at the boiling point for 30 min. After that, it was rinsed, and then dried at 100°C for 1 h.

Coating Procedure

The coating was conducted in an atmosphere-controlled sealed furnace with a volume of ~1.2 L. It was designed as shown in Scheme 1. There are two electrically heating panels in this reactor. The bottom heating panel creates the decomposition temperature (T_1) and the top one is used to produce the oxidative deposition temperature (T_2). The exact temperatures (T_1, T_2) were controlled independently by thermocouples. The substrate was placed on the support plate. A gap ($d = 0$ or ~3 mm) can be made between the substrate and the top heating panel. In a typical experimental process, the as-prepared bulk silicone was cut into irregular particles and then the particles were scattered on the bottom heating panel as uniform as possible. Following, the mixture gas of oxygen and nitrogen (the volume ratio of O_2/N_2 was ~1 : 4) flowed into the reactor and then stopped. The values of T_1 and T_2 were changed with a rising rate of ~30°C·min^{-1}. The deposition was lasted for about 3 h.

Characterizations

Water contact angles (WCAs) were characterized by using a DropMeter™ A-100P equipped with a CCD camera. (MAIST Vision Inspection & Measurement, China). Static WCAs were measured with a 4 μL Milli-Q water droplets. The average contact angle was obtained by measuring more than five different positions on the same sample. Field emission scanning electron microscopy (FESEM, Hitachi, S-4800) was used to investigate the surface morphologies of the coatings. Fourier transform infrared (FT-IR) spectra were recorded on a FT-IR spectrometer (Nicolet Nexus670). Ultraviolet (UV)–Vis–NIR spectra were collected at normal incidence with a UV-3101PC (SHIMADZU,

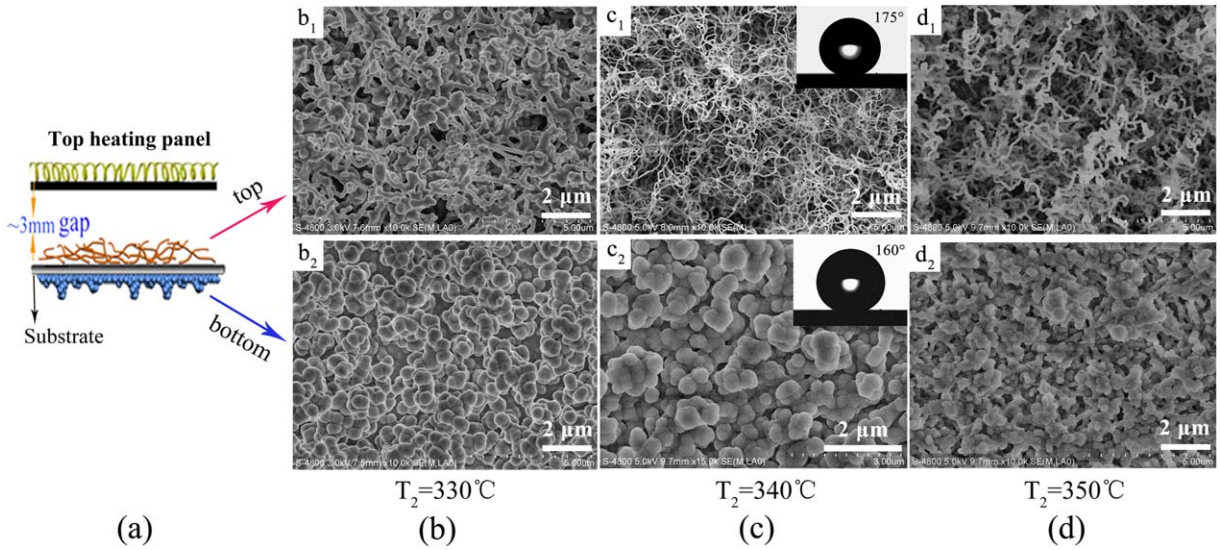

Figure 1. (a) Schematic for the preparation of the coatings on both sides of the glass substrates. A gap of ~3 mm was made between the subtrate and the top heating panel (d = ~3 mm). (b)-(d) FESEM images of the samples which were prepared with 0.5 g bulk silicone at $T_1 = 320°C$, $T_2 = 330$, 340, and 350°C, respectively. (b_1, c_1, d_1) and (b_2, c_2, d_2) show SEM images of the top and bottom surfaces, respectively. The insets in Figure 6(c_1,c_2) show the microphotographs of WCAs of the corresponding coatings. [Color figure can be viewed in the online issue, which is available at wileyonlinelibrary.com.]

Japan) in double-beam mode. Raman spectra in a range of 200–2500 cm^{-1} were recorded by a Labram HR800 (Jobin Yvon, France). Thermogravimetry-differential thermal analysis (TG-DTA) was performed with a thermal analysis system (Diamond TG/DTA, PERKIN-ELMER) at 10°C·min^{-1}. Photoluminescence (PL) spectra were measured using a fluorescence spectrophotometer (Horiba Jobin Yvon, France) at room temperature. XPS experiment was performed by using an ESCAlab MK2 X-ray photoelectron spectroscopy (Vaccum Generator Scientific, UK).

RESULTS AND DISCUSSION

Figure 1 shows the FESEM images of the silicone–carbon composite coatings, which were prepared with 0.5 g bulk silicone at $T_1 = 320°C$ but at different deposition temperatures. As shown in Figure 1(a), 3-mm gap was made between the substrate and the top heating panel so that the components of the thermal decomposition can be deposited on both of the surfaces of the substrates. The results indicate that the morphologies are closely related to the self-aggregation conditions. The sample prepared at $T_2 = 330°C$ showed the short fibers with an average diameter of ~250 nm covered on the top surface and some papillae composited in the short fibers [Figure 1(b_1)], whereas the bottom surface was covered by papillae with a length of ~ 2μm [Figure 1(b_2)], which were self-organized by several particles at a size of ~300 nm. When T_2 is 340°C, the tortuous long nanofibers with a diameter of ~80 nm on the top surface, and uniform ~500 nm papillae were obtained on the bottom surface, [Figure 1(c_1,$1c_2$)]. Figure 1(d_1–d_2) show the SEM images of the sample prepared at $T_2 = 350°C$. The morphologies are similar to that of the sample prepared at $T_2 = 340°C$. Either the nanofibers or papillae were formed by the self-aggregation of the silicone–carbon composite nanoparticles. The as-prepared coatings both on the top and the bottom surface all possess superhydrophobicity. The typical WCAs values for both surfaces are 175° and 160°, respectively [see the insets in Figure 1(c_1,c_2)]. For a comparison of Figure 1(b–d), the results demonstrated that the more uniform long fibers and more ordered structures can be obtained at higher deposition temperature.

Oxygen gas is also a very important factor in the formation of the morphologies, wettability, as well as the optical properties of the silicone–carbon composite coatings including color, and transparency. The black, brown, yellow, and colorless samples coated only on the bottom surface with different superhydrophobicity were prepared at $T_1 = 320°C$, and $T_2 = 350°C$ with 5.0 g, 3.0 g, 2.0 g, and 0.25 g bulk silicone, respectively. No gap exists between the substrates and top heating panel (d = 0 mm). The relative concentration of gaseous oxygen in the sealed reactor decreased and the sample colors became deeper with more bulk silicone decomposed. Therefore, the colored samples could be achieved under an oxygen-deficient atmosphere. UV–Vis–NIR spectra of the four samples are shown in Figure 2. The results indicated that the black sample absorbs nearly all light in the visible region, whereas it shows some degree of transparency in the NIR region. The brown sample shows high transmittance in the region of 750–2500 nm while it decreases sharply in the visible region. The yellow sample shows a broad absorption band at about 680 nm, and the colorless sample shows high transmittance in the region of 400–2500 nm.

Figure 3(a–c) show FESEM images of the microstructured surfaces from the black, yellow, and colorless samples, respectively. Figure 3(a) shows that the surface of the black sample was covered by flocs, which were formed by self-aggregation of about 100 nm particles. Unlike the morphology of the black sample, papillae can be observed from the images of the yellow and colorless samples, as shown in Figure 3(b,c). The sizes of the

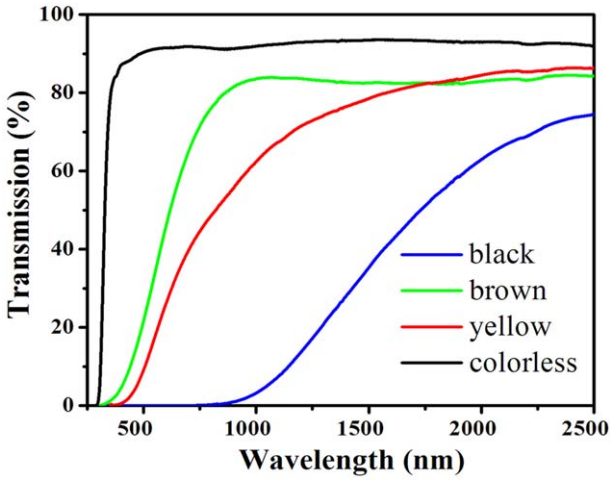

Figure 2. UV–Vis–NIR spectra of the black, brown, yellow, and colorless coatings on glass substrates. The black, brown, yellow, and colorless samples were prepared at $T_1 = 320°C$, $T_2 = 350°C$ using 5.0 g, 3.0 g, 2.0 g, and 0.25 g bulk silicone, respectively. No gap exists between the substrates and top heating panel ($d = 0$ mm). [Color figure can be viewed in the online issue, which is available at wileyonlinelibrary.com.]

papillae coated on the yellow sample (1–2 μm) are significantly larger than those on the colorless one (200–400 nm), which can be attributed to the increased diameter of the self-aggregation particles. The WCAs measured for the black, yellow, and colorless samples are 167°, 156°, and 155°, respectively, demonstrating these coated surfaces possess superhydrophobicity [see Figure 3(a–c) insets]. Figure 3(d) shows the SEM image of the coating prepared at $T_1 = 320°C$, and $T_2 = 350°C$ with 0.1 g bulk silicone, from which we could observe that some of the papillae were destroyed and the corresponding WCA value was only up to 123° [see Figure 3(d) inset]. Thus, the wettabilities of the silicone–carbon composite coatings are also strongly related to the concentration of gaseous oxygen.

Figure 4 shows Raman spectra of the colorful samples. The peaks for the strong C—C vibrations (D band at ~1330 cm^{-1}, and G band at ~1600 cm^{-1}) can be observed on the black [Figure 4(a)] and brown [Figure 4(b)] samples. Moreover, the peaks observed on the black sample are much stronger than that of the brown one, and no obvious peaks can be observed on the colorless sample [Figure 4(c)]. The results imply that the amorphous carbons exist in the colored coatings. The results are also consistent with the XPS spectra (Figure 5).

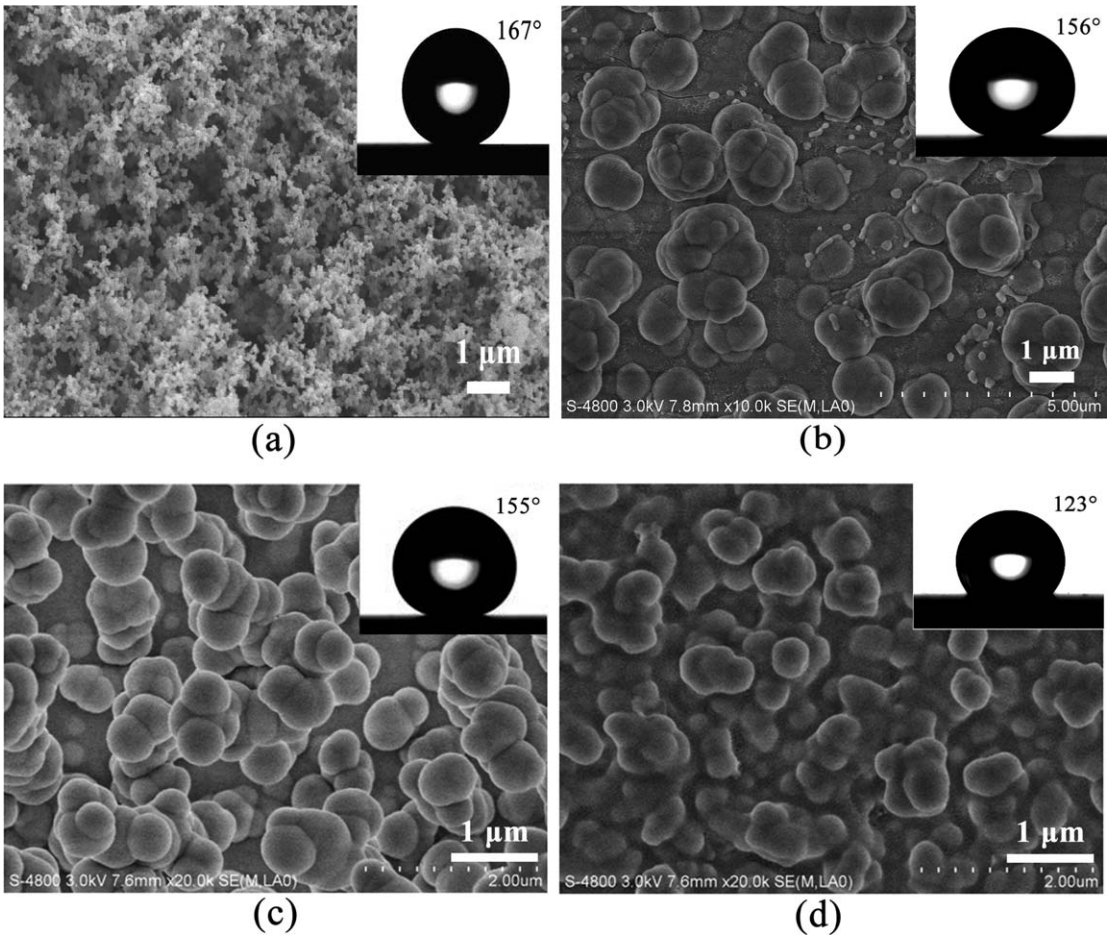

Figure 3. FESEM images of the superhydrophobic black (a), yellow (b), and colorless (c), and less hydrophobic (d) coatings on glass substrates. The less hydrophobic samples were prepared at $T_1 = 320°C$, $T_2 = 350°C$ using 0.1 g bulk silicone. Insets show the microphotographs of WCAs of the corresponding coatings.

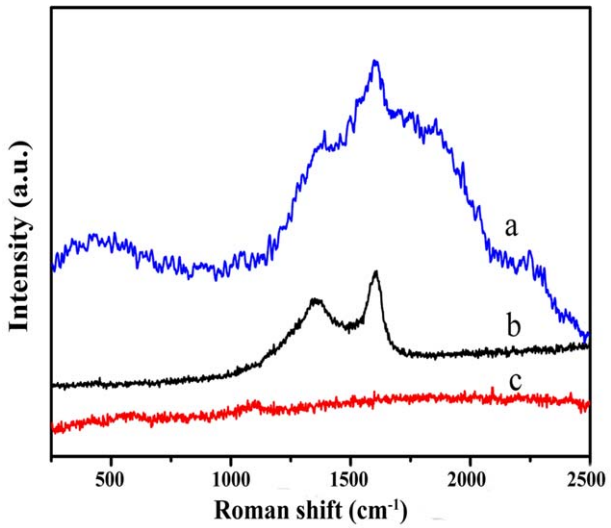

Figure 4. Raman spectra of the black (a), brown (b), and colorless (c) samples. [Color figure can be viewed in the online issue, which is available at wileyonlinelibrary.com.]

Figure 5(a) shows the XPS survey of the black sample. It reveals the existence of silicon (Si 1s, 150 eV, Si 2p, 100 eV), carbon (C 1s, 284 eV), and oxygen (O 1s, 532 eV). Figure 5(b) demonstrates the XPS spectrum of C 1s. The measured spectrum can be resolved into two peaks, corresponding to sp^3 (C—H, and C—C) at binding energy of 285.3 eV and C—Si at 284.4 eV. XPS spectrum of the Si 2p was also measured, as shown in Figure 5(c). It can be resolved into three peaks: Si—C at 100.8 eV, Si—O—Si at 101.4 eV, and Si—OH at 102.5 eV. The material compositions of the coatings as determined by the XPS are in good agreement with FT-IR results (see Figure 6).

Figure 6 shows the FT-IR spectra of the black, brown and colorless samples. The absorption peak centered at around 1100 cm^{-1} is caused by Si—O—Si asymmetric stretching vibration [28,29]. The peak centered at around 1626 cm^{-1} and the broad absorption band at around 3440 cm^{-1} are due to the O—H groups.[28] And the absorption bands observed at around 1280 and 2980 cm^{-1} are attributed to bending and stretching of C—H bonds and the peaks observed at 855 cm^{-1} are due to the

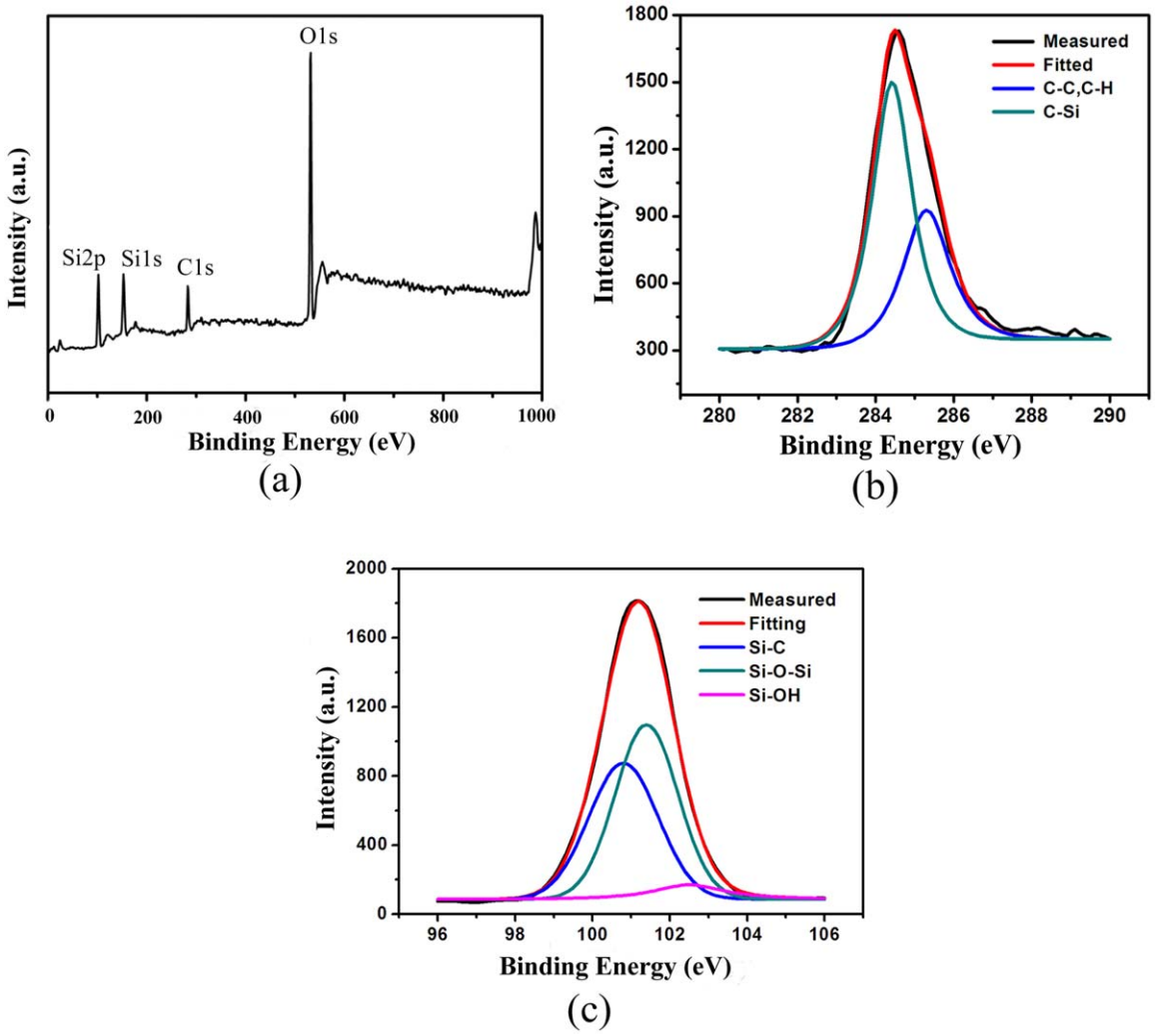

Figure 5. XPS spectra of (a) the black sample, (b) C 1s, and (c) Si 1s, respectively. [Color figure can be viewed in the online issue, which is available at wileyonlinelibrary.com.]

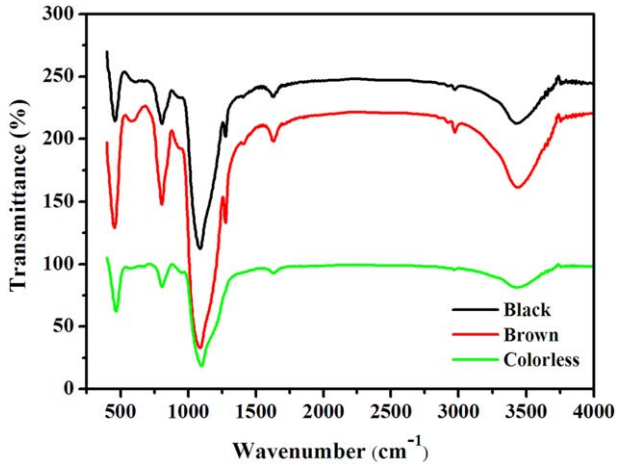

Figure 6. FT-IR spectra of the black, brown, and colorless samples. [Color figure can be viewed in the online issue, which is available at wileyonlinelibrary.com.]

Si—C bonds.[28] The result suggests that the alkyl and hydroxyl groups are co-existed in the coatings.

Figure 7(a) shows the PL spectra of the black, brown, yellow, and colorless samples, which were excited by the wavelength of 372 nm. The results reveal that the colored samples demonstrate obvious fluorescence in the blue-light region. In addition, the colored samples show multicolor emission in the visible region. For example, if the excitation wavelengths were selected at 410, 460, and 500 nm, the corresponding emission spectra of the yellow sample are red-shifted, and the peaks were, respectively, centered at 475, 525, and 550 nm [see Figure 7(b)]. However, the PL intensity decreases as the PL peak red-shifted. This is a common phenomenon observed in carbon-based dots.[30] Therefore, the colors and PL of the silicone–carbon composite coatings should be contributed to carbons embedded inside the coatings.

The bulk silicone is unstable at higher temperature. Figure 8(a) shows the TG-DTA curve of the bulk silicone under nitrogen flow. Before 200°C, the TG curve shows a weight loss of about 40% while there is no obvious exothermic peak in DTA, which could be attributed to the post-condensation of unreacted Si—OH bonds to form Si—O—Si bonds and the loss of low molecule-weight silicone oil. The cleavage of Si—O—Si network structures and Si—C bond, which occurred between 200 and 550°C, were accompanied by a board exothermic peak in the DTA curve with a maximum at ~500°C and with a weight loss of ~50%. The total weight loss is ~90% as given by the TG curve, indicating the bulk silicone can mostly be decomposed under high temperature in a nitrogen atmosphere. However, no superhydrophobic coating but only black silicone oil was formed by oCVD. The TG-DTA analysis of the bulk silicone under oxygen flow was also investigated, as shown in Figure 8(b). Compared to Figure 8(a), some differences could be observed. In the region from 200 to 500°C, the cleavage of Si—O—Si network structures and Si—C bond occurred with a weight loss of ~20%, and they were accompanied, respectively, by a broad exothermic peak at 340°C and a sharp exothermic peak at 450°C. The total weight loss is ~55%. The results closely agree with the investigation of the thermal behavior of the silicon resin which reported by Jancke et al.[31] Thus, oxygen gas played a crucial role in our experiments. Although the mechanisms of this route cannot be known very well now, we considered that the bulk silicone was thermo-oxidative decomposed by parts of the Si—O—Si network structures and Si—C bonds. The Si—O—Si network structures would be oxidized to silicate structures, while Si—C bonds cleave by an oxidative conversion to Si—OH bonds. The organic substituents methyl and ethyl could be pyrolysed to form carbons (see the Raman spectra in Figure 4) in varying degrees depending on the content of gaseous oxygen, which result in the coatings possess different colors and fluorescence (see Figures 2 and 7, respectively). When the content of gaseous oxygen is enough, lots of new formed Si—OH bond causes the prepared coatings no longer superhydrophobic any more. However, in a relative oxygen-deficient atmosphere, the as-prepared coatings with a bit of

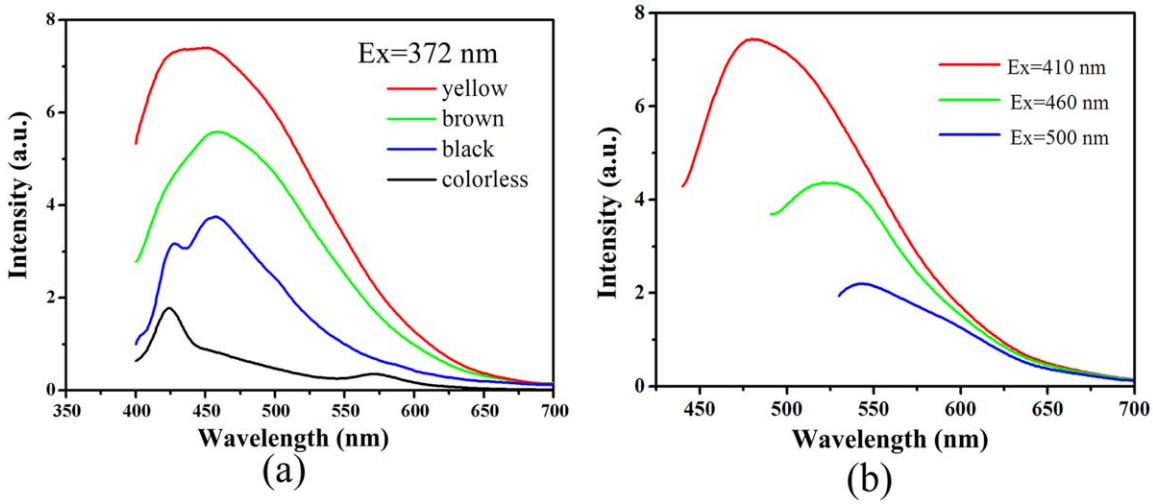

Figure 7. PL emission spectra of (a) the black, brown, yellow, and colorless samples excited by 372 nm; (b) the yellow sample excited by various wavelengths. [Color figure can be viewed in the online issue, which is available at wileyonlinelibrary.com.]

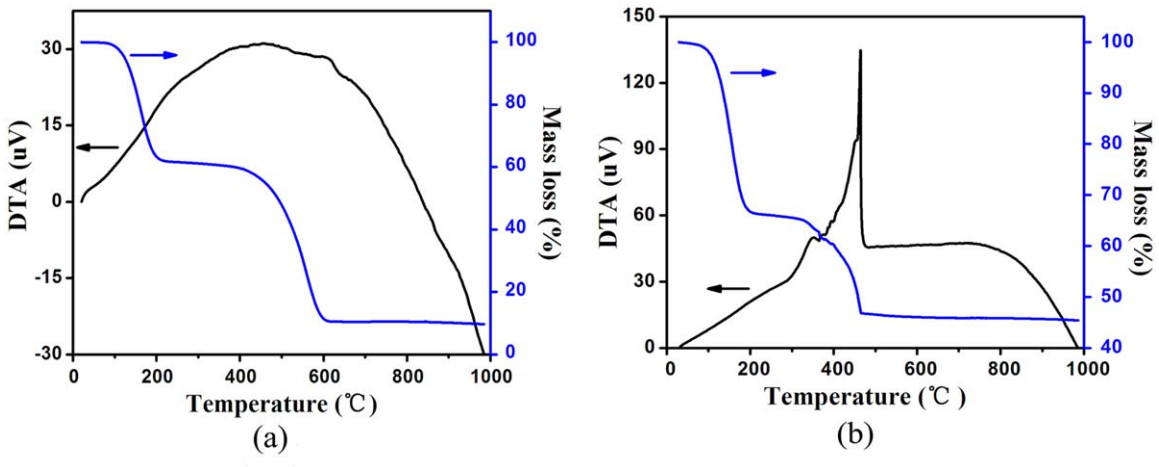

Figure 8. Thermogravimetry-differential thermal analysis (TG-DTA) of silicone under (a) N_2 and (b) O_2 flow. [Color figure can be viewed in the online issue, which is available at wileyonlinelibrary.com.]

Si—OH bond in the surface are still superhydrophobic which mainly responsible for the micro-nanostructure and lots of hydrophobic organic groups which still attached on the network structure, as the scheme shown in Figure 9(a). Figure 9(b) shows the photograph of about 40-μL water drops on a glass slide with highly transparent superhydrophobic coating. Nearly sphere-like water droplets were formed. The solid–liquid interfacial interaction is extremely weak, as demonstrated in Figure 9(c), a water droplet of 5 μL, suspending on the tip of a syringe, is difficult to be placed on the hydrophobic surface, even though the droplet is deformed severely.

Our facile method of preparing multifunctional silicone–carbon composite coatings by one-step thermal decomposition of cheap bulk silicone has not been reported yet. More interestingly, the nanofibers were formed on the top surface when a gap was existed between the substrate and the top heating panel. The strategy to direct the thermal decomposed components or the silicone vapor into the gap plays an important role, because no nanofibers can be found on the bottom surfaces under various experimental conditions. The detailed mechanism is not well understood. But it must be different from that of the silicone nanofilaments which were achieved by the hydrolysis and condensation of reactive organosilanes.[23,24] Because the nanofibers we prepared here are formed by the self-aggregation of the silicone–carbon composite nanoparticles. As known, the mechanism of growing nanostructures could be attributed to potential kinetic effects during oCVD, which also should govern the growth of our micro/ nanostructures.

Our highly transparent superhydrophobic coatings can be applied to anti-wetting window glass or rear-view mirrors of cars. Additionally, the superhydrophobic coatings could have another application, providing an approach to obtain small

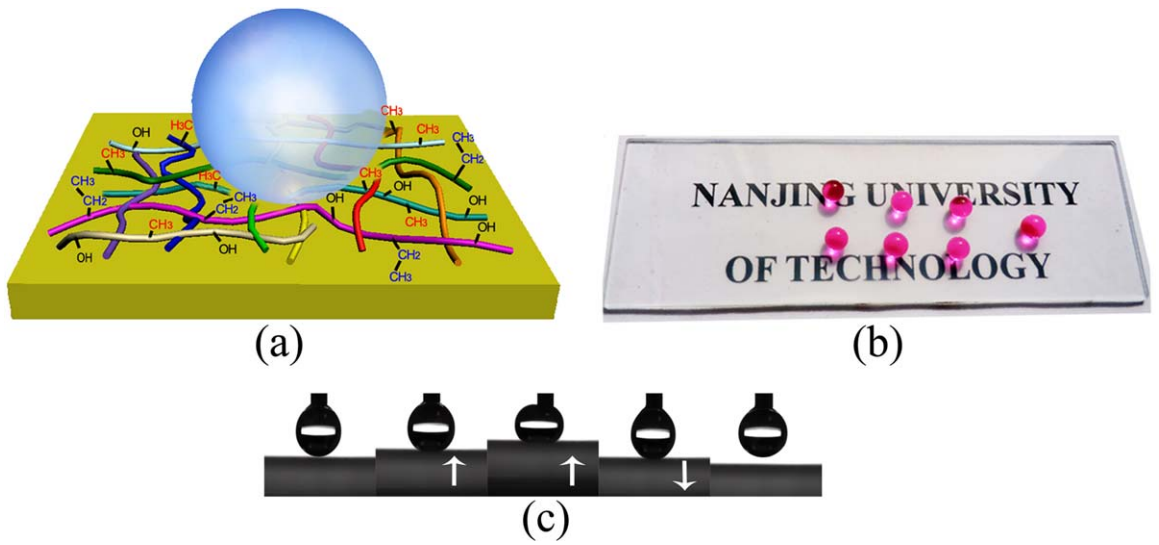

Figure 9. (a) Schematic of a water drop on the superhydrophobic silicone–carbon composite nanofibers coating; (b) Photograph of water drops on the transparent colorless sample with high superhydrophobicity; (c) Approach, contact, deformation, and departure processes of a water droplet suspended on a syringe with respect to the coating surfaces. The arrows represent the moving direction of the substrate. [Color figure can be viewed in the online issue, which is available at wileyonlinelibrary.com.]

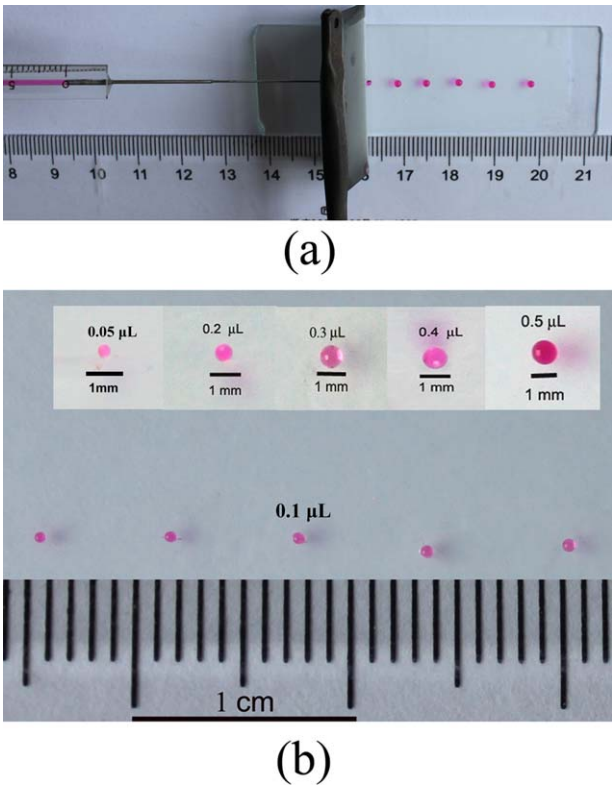

Figure 10. Photographs of the individual water droplets prepared by cutting down water droplets from the tip of the micro-syringe onto a superhydrophobic substrate using a superhydrophobic thin iron blade. (a) 2.0 μL, (b) 0.05, 0.1, 0.2, 0.3, 0.4, and 0.5 μL The water here was red-colored by the rhodamine B dye for easy observation. [Color figure can be viewed in the online issue, which is available at wileyonlinelibrary.com.]

water drops, particularly in nanoliter scales. As known, generating a tiny drop is easy through micro-syringe, however, it is difficult to cling to the superhydrophobic surface independently due to the strong capillary action between the drop and the tip of the syringe [Figure 9(c)]. Superhydrophobic knife[32] can solve the problem, and here we also prepared a superhydrophobic knife by coating on both sides of a thin blade, as shown in Figure 10(a). By using this superhydrophobic knife, water droplets of 0.05, 0.1, 0.2, 0.3, 0.4, and 0.5 μL can successfully stay on the superhydrophobic surface from the tip of a syringe, as shown in Figure 10(b). Therefore, this method can be used to achieve individual tiny water drop one by one with different sizes, which could be applied in microreactors or microfluid system. On the other hand, photoluminescent carbon has drawn increasing attention due to their potential applications in biomedical imaging, photovoltaics, catalysis, and optical-power limiting.[33–36] It's desirable to embed them in an appropriate solid matrix or prepare in solid-state architectures in real device applications.[37] Our method can provide photoluminescent carbon embedded in a solid-state architecture within one-step process. This may be easily applied in photo-functional devices.

CONCLUSIONS

A facile one-step oCVD method was presented to fabricate micro-nanostructured superhydrophobic silicone–carbon composite coatings with transparency, colors, and fluorescence. Oxygen gas is of great important to the multifunctional properties of the silicone–carbon composite coatings. With this solvent-free process, we could prepare the black, brown, and yellow silicone–carbon composite coatings with different wettability and transparency under oxygen-deficient atmospheres. These colored coatings showed PL in the blue light region when they were excited by UV light, which could be attributed to carbons embedded inside the silicone–carbon composite coatings. Furthermore, instead of the fluorine-containing reagents or reactive organosilanes, we use the cheap environmental-friendly bulk silicone as our raw material. It was no doubt that the superhydrophobic coatings with multifunction would enlarge the applications of anti-wetting materials.

ACKNOWLEDGMENTS

This work was supported by the National Natural Science Foundation of China (20573055, 21071081) and a Project Funded by the Priority Academic Program Development of Jiangsu Higher Education Institutions of China.

REFERENCES

1. Deng, X.; Mammen, L.; Zhao, Y.; Lellig, P.; Müllen, K.; Li, C.; Butt, H. J.; Vollmer, D. *Adv. Mater.* **2011**, *23*, 2962.
2. Kamegawa, T.; Shimizu, Y.; Yamashita, H. *Adv. Mater.* **2012**, *24*, 3697.
3. Sarkar, D. K.; Saleema, N. *Surf. Coat. Technol.* **2010**, *204*, 2483.
4. Steele, A.; Bayer, I.; Loth, E. *J. Appl. Polym. Sci.* **2012**, *125*, 445.
5. Jiang, C.; Zhang, Y.; Wang, Q.; Wang, T. *J. Appl. Polym. Sci.* **2013**, *129*, 2959.
6. Wang, Y.; Lu, N.; Xu, H.; Shi, G.; Xu, M.; Lin, X.; Li, H.; Wang, W.; Qi, D.; Lu, Y.; Chi, L. *Nano Res.* **2010**, *3*, 520.
7. Li, Y.; Zhang, J.; Zhu, S.; Dong, H.; Jia, F.; Wang, Z.; Tang, Y.; Zhang, L.; Zhang, S.; Yang, B. *Langmuir* **2010**, *26*, 9842.
8. Yao, X.; Song, Y.; Jiang, L. *Adv. Mater.* **2011**, *23*, 719.
9. Camargo, K. C.; Michels, A. F.; Rodembusch, F. S.; Horowitz, F. *Chem. Commun.* **2012**, *48*, 4992.
10. Ishizaki, T.; Sakamoto, M. *Langmuir* **2011**, *27*, 2375.
11. Ogihara, H.; Okagaki, J.; Saji, T. *Langmuir* **2011**, *27*, 9069.
12. Xue, C. H.; Zhang, P.; Ma, J. Z.; Ji, P. T.; Li, Y. R.; Jia, S. T. *Chem. Commun.* **2013**, *49*, 3588.
13. Li, X.; Du, X.; He, J. *Langmuir* **2010**, *26*, 13528.
14. Ghosh, N.; Bajoria, A.; Vaidya, A. A. *ACS Appl. Mater. Interfaces* **2009**, *1*, 2636.
15. Xu, Q. F.; Wang, J. N.; Sanderson, K. D. *ACS Nano* **2010**, *4*, 2201.
16. Zhang, J.; Seeger, S. *Adv. Funct. Mater.* **2011**, *21*, 4699.
17. Zhang, J.; Seeger, S. *Angew. Chem. Int. Ed.* **2011**, *50*, 6652.
18. Li, X. Y.; Du, X.; He, J. H. *Langmuir* **2010**, *26*, 13528.
19. Zhang, J. P.; Seeger, S. *Chemphyschem* **2013**, *14*, 1646.

20. De Givenchy, E. T.; Amigoni, S.; Martin, C. D.; Andrada, G.; Caillier, L.; GéRibaldi, S.; Guittard, F. D. R. *Langmuir* **2009**, *25*, 6448.

21. Zimmermann, J.; Rabe, M.; Artus, G. R. J.; Seeger, S. *Soft Mater* **2008**, *4*, 450.

22. Gao, L. C.; Mccarthy, T. J. *J. Am. Chem. Soc.* **2006**, *128*, 9052.

23. Artus, G. R. J.; Jung, S.; Zimmermann, J.; Gautschi, H. P.; Marquardt, K.; Seeger, S. *Adv. Mater.* **2006**, *18*, 2758.

24. Artus, G. R. J.; Seeger, S. *Ind. Eng. Chem. Res.* **2011**, *51*, 2631.

25. Zhang, Y. M.; Huang, Y.; Liu, X. L.; Yu, Y. Z. *J. Appl. Polym. Sci.* **2003**, *89*, 1702.

26. Yang, L.; Hu, Y.; Lu, H.; Song, L. *J. Appl. Polym. Sci.* **2006**, *99*, 3275.

27. Pol, V. G.; Pol, S. V.; Gedanken, A.; Lim, S. H.; Zhong, Z.; Lin, J. *J. Phys. Chem. B* **2006**, *110*, 11237.

28. Latthe, S. S.; Imai, H.; Ganesan, V.; Venkateswara Rao, A. *Micropor. Mesopor. Mater.* **2010**, *130*, 115.

29. Rao, A. V.; Gurav, A. B.; Latthe, S. S.; Vhatkar, R. S.; Imai, H.; Kappenstein, C.; Wagh, P. B.; Gupta, S. C. *J. Colloid Interface Sci.* **2010**, *352*, 30.

30. Tang, L.; Ji, R.; Cao, X.; Lin, J.; Jiang, H.; Li, X.; Teng, K. S.; Luk, C. M.; Zeng, S.; Hao, J.; Lau, S. P. *ACS Nano.* **2012**, *6*, 5102.

31. Jancke, H.; Schultze, D.; Geissler, H. In Organosilicon Chemistry II; Auner, N.; Weis, J., Eds.; Wiley: Burghausen, **2008**; Chapter *84*, p 697.

32. Yanashima, R.; Garcia, A. A.; Aldridge, J.; Weiss, N.; Hayes, M. A.; Andrews, J. H. *Plos One* **2012**, 7.

33. Liu, R.; Wu, D.; Liu, S.; Koynov, K.; Knoll, W.; Li, Q. *Angew. Chem.* **2009**, *121*, 4668.

34. Li, Q.; Ohulchanskyy, T. Y.; Liu, R.; Koynov, K.; Wu, D.; Best, A.; Kumar, R.; Bonoiu, A.; Prasad, P. N. *J. Phys. Chem. C* **2010**, *114*, 12062.

35. Peng, J.; Gao, W.; Gupta, B. K.; Liu, Z.; Romero-Aburto, R.; Ge, L.; Song, L.; Alemany, L. B.; Zhan, X.; Gao, G.; Vithayathil, S. A.; Kaipparettu, B. A.; Marti, A. A.; Hayashi, T.; Zhu, J.-J.; Ajayan, P. M. *Nano Lett.* **2012**, *12*, 844.

36. Gu, F.; Ren, X.; Zhang, J.; Shao, W.; Huang, G.; Li, C. *Ind. Eng. Chem. Res.* **2011**, *50*, 12542.

37. Wang, F.; Xie, Z.; Zhang, H.; Liu, C. Y.; Zhang, Y. G. *Adv. Funct. Mater.* **2011**, *21*, 1027.